THE JOURNAL OF PHYSICAL CHEMISTRY C

Article

pubs.acs.org/JPCC

Carbon Nanostructured Fibers As Counter Electrodes in Wire-Shaped Dye-Sensitized Solar Cells

Shaowu Pan,[†,‡] Zhibin Yang,[‡] Peining Chen,[‡] Xin Fang,[‡] Guozhen Guan,[‡] Zhitao Zhang,[‡] Jue Deng,[‡] and Huisheng Peng*[,†,‡]

[†]School of Materials Science and Engineering and Institute for Advanced Materials and Nano Biomedicine, Tongji University, 4800 Caoan Road, Shanghai 201804, China

[‡]State Key Laboratory of Molecular Engineering of Polymers, Department of Macromolecular Science, and Laboratory of Advanced Materials, Fudan University, 2205 Songhu Road, Shanghai 200438, China

Supporting Information

ABSTRACT: Carbon nanotubes (CNT), core−sheath CNT/reduced graphene oxide nanoribbon (RGONR), CNT/RGO composite, and RGO fibers have been compared as counter electrodes to fabricate novel dye-sensitized solar cells. For the I^-/I_3^- electrolyte, the core−sheath CNT/RGONR fiber shows the best catalytic activity, which in turn produces the highest energy conversion efficiency of 5.64%. In contrast, for the organic T^-/T_2 electrolyte, the highest energy conversion efficiency has been produced from the CNT fiber counter electrode with the maximal value of 4.78%. The different electrocatalytic activities among these four carbon nanostructured fibers on the two typical electrolytes of I^-/I_3^- and T^-/T_2 have been carefully investigated in this work.

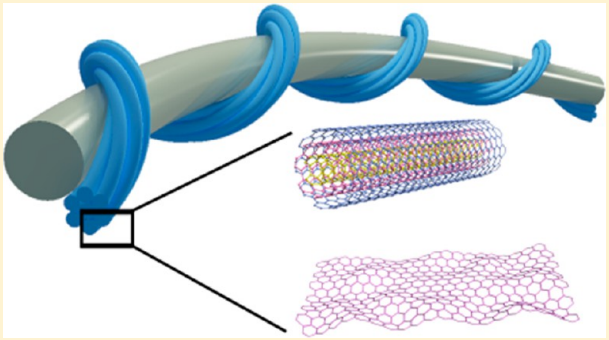

INTRODUCTION

With the rapid advancement in microelectronic technology, miniaturized electronic products have attracted increasing attention and may dominate our life in the near future. To this end, it is necessary to develop miniature power systems[1−4] such as solar cells[5,6] with low cost, high efficiency, light weight, and high flexibility as the conventional silicon-based technologies cannot effectively meet them. The silicon-based solar cells[7] are generally produced under high vacuum and appear in heavy plates. In contrast, dye-sensitized solar cells (DSCs),[8] the next-generation photovoltaic devices, were fabricated by an easy solution process and could also be made into flexible structures.[9−11] In addition, DSCs had currently achieved high energy conversion efficiencies up to 12.3%.[12] Therefore, the development of high-performance DSCs represents a new and general strategy to solve the above problem.

A typical DSC is composed of a working electrode, counter electrode, and electrolyte. The working electrode has been generally prepared by coating a dye-sensitized nanoporous TiO_2 film on a transparent conductive substrate, while the counter electrode is formed by depositing a thin layer of platinum film also on a conductive substrate.[13] The two electrodes play critical roles on the photovoltaic performances of DSCs; for example, the catalytic activities of counter electrodes greatly affect the short-circuit currents.[14,15] A redox couple of I^-/I_3^- is mostly studied as the electrolyte due to the low cost and easy preparation. However, some obvious disadvantages including low stability (it is corrosive to the metal-based current collectors such as copper and silver, and iodine may be easily sublimated) and absorption to the visible light[16] may have greatly limited the practical application. Therefore, many efforts had also been paid to find alternative redox couples[17−19] such as Co_3^+/Co_2^+, TEMPO/TEMPO$^+$, T^-/T_2, and Br^-/Br_3^-. Among them, the organic T^-/T_2 electrolyte had recently attracted extensive attention because it is noncorrosive with negligible light absorption.[20] This organic electrolyte is particularly promising to the flexible DSCs for various portable electronic devices.

It is also critical to match the counter electrode according to the electrolyte to further improve the photovoltaic performances of DSCs. In other words, the same counter electrode may demonstrate different catalytic activities on different electrolytes. For instance, platinum has been widely explored for a high catalytic activity in the I^-/I_3^- electrolyte, although it showed a much lower activity on the T^-/T_2 electrolyte.[21,22] Besides the conventional platinum electrode, many efforts have been recently paid to develop other electrode materials including conductive polymers[23−25] (e.g., poly (3,4-ethylenedioxythiophene), polyaniline, and polypyrrole), carbon materials[26−28] (active carbon, mesoporous carbon, carbon

Special Issue: Michael Grätzel Festschrift

Received: October 21, 2013
Revised: November 26, 2013

   dx.doi.org/10.1021/jp410402w | J. Phys. Chem. C XXXX, XXX, XXX−XXX

nanotube (CNT), and graphene), and inorganic compounds.[29,30] In particular, carbon nanomaterials such as CNT[31,32] and graphene were mostly investigated for promising candidates due to large surface areas and remarkable electronic and catalytic properties.[33]

Currently, the DSCs are generally made into planar structures that remain challenging to many portable electronic facilities such as wearable devices. To this end, wire-shaped DSCs have been recently proposed with unique and promising advantages of being lightweight and woven into textiles[34,35] (similar to the chemical fibers) compared with the conventional planar structure. In a typical fabrication, two fibers as working and counter electrodes are twisted together to form the wire-shaped DSCs.[36−38] The electrolyte is infiltrated into two fiber electrodes and among them. Similar to the film-structured DSCs, the selection of the matching fiber counter electrode and electrolyte is critically important to produce high energy conversion efficiencies in DSCs, although it remains unavailable for a systematical study.

Herein a family of carbon nanostructured fibers based on CNT and reduced graphene oxide (RGO) has been studied as counter electrodes to fabricate wire-shaped DSCs with the same Ti wire working electrode. The core−sheath CNT/RGONR fiber was found to exhibit the highest energy conversion efficiency for the I^-/I_3^- electrolyte, while the bare CNT fiber produced the highest energy conversion efficiency for the T^-/T_2 electrolyte. For both I^-/I_3^- and T^-/T_2 electrolytes, the RGO fiber showed the lowest energy conversion efficiency mainly due to a low electrical conductivity.

EXPERIMENTAL SECTION

1. Materials and Reagents. Phosphoric acid, sulfuric acid, potassium permanganate, hydrogen peroxide (30% in water), hydrogen iodide, ethylene glycol, iodine, and calcium chloride were all obtained from Sinopharm Chemical Reagent, China. Graphite powder (diameter of 40 μm) was ordered from Qingdao Henglide Graphite, China. Ammonium fluoride and 5-mercapto-1-methyltetrazole were provided by Aladdin Reagent, China. Titanium wire (diameter of 127 μm), platinum wire (diameter of 25 μm), and ethylene carbonate were obtained from Alfa. Tetramethylammonium hydroxide (10% in methanol) was ordered from TCI. The dye of N719, that is, $RuL_2(NCS)_2$ (L = 4,4′-dicarboxylate-2, 2′-bipyridine), was provided by Heptachroma, China. The synthesis of the organic redox couple of T^-/T_2 (Scheme 1) was described elsewhere.[22]

Scheme 1. Structure of Redox Couple (T^- and T_2)

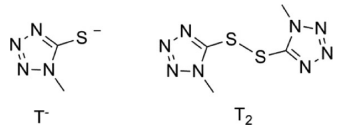

2. Synthesis of Carbon Nanostructured Fibers. Spinnable CNT arrays that were synthesized by a chemical vapor deposition in a quartz tube furnace were previously reported,[39] and the used arrays showed a thickness of ∼300 μm in this work. CNT fibers had been then dry-spun from the arrays with a speed of 2000 rpm (Figure S1 in the Supporting Information).

To synthesize the core−sheath CNT/reduced graphene oxide nanoribbon (RGONR) fiber, we first prepared a mixture from 4 mL of H_3PO_4 (85%) and 36 mL of concentrated H_2SO_4, followed by the addition of 40 mg of $KMnO_4$ under stirring for 15 min until the solution turned emerald green. The spun CNT fibers were then immersed into the mixture solutions, followed by heating at 75 °C for 1 h to unzip CNT into graphene oxide nanoribbon (GONR).[40,41] The resulting fiber was carefully washed successively by 30% H_2O_2 and deionized water. The reduction of GONR was made in an HI aqueous solution (45 wt %) at 80 °C in dark for 8 h, followed by washing with deionized water and drying for 12 h in air.

GO sheets were first synthesized according to the previous procedures to synthesize CNT/RGO composite fibers.[42] The GO solution in ethanol was then obtained by mixing a GO solution in deionized water (1.4 wt %, 0.5 mL) with ethanol (10 mL). CNT sheets that were dry-drawn from the spinnable CNT arrays were fixed onto glass slides by one end with the other one connected to a rotate tip at a speed of 2000 rpm. The GO ethanol solution was dropped onto the triangle zone (similar to the labeled area in Figure S1 in the Supporting Information) to form CNT/GO composite fibers. The dried fibers were also reduced in the HI aqueous solution (45 wt %) at 80 °C in dark for 8 h, followed by washing with deionized water and drying for 12 h in air.

The RGO fibers were synthesized by chemical reduction of GO fibers. The GO fibers were prepared through a wet-spinning method by injecting a GO dispersion (2 wt %) into a coagulation bath with an injecting speed of 100 μL/min (diameter of syringe needle, 410 μm). The coagulation bath was composed of 5 wt % $CaCl_2$ solution in ethanol/water (1:3 v/v). After immersion in the coagulation bath for 30 min, the GO fibers were transferred into ethanol and water baths to remove the residual coagulation solution and dried at room temperature. The RGO fibers were then obtained by reducing the GO fibers in the HI aqueous solution (45 wt %) at 80 °C for 8 h, followed by washing with ethanol and drying for 12 h.

3. Fabrication of Wire-Shaped Dye-Sensitized Solar Cells. TiO_2 nanotube arrays were synthesized by electrochemical anodization of Ti wires in a fluoride-containing electrolyte. Ti wires were sonicated successively in acetone and isopropyl and then rinsed with ethanol before drying. Typically, the anodization occurred at 0.3 wt % NH_4F/ethylene glycol solution containing 8 wt % H_2O and a voltage of 60 V in a two-electrode electrochemical cell with a Pt sheet as a counter electrode for 6 h. The anodized Ti wires were rinsed with deionized water and then annealed in air at 500 °C for 1 h. They were then immersed in a 0.1 M $TiCl_4$ aqueous solution at 70 °C for 30 min and annealed again in air at 450 °C for 0.5 h. The treated wires were cooled to 120 °C before being immersed in a 0.3 mM N719 solution of dehydrated acetonitrile and *tert*-butanol (v/v 1/1) for 16 h. The carbon nanostructured fiber was twisted around the dye-absorbed working electrode with a screw pitch of ∼1 mm to form wire-shaped DSCs. For the convenience of measurements, the resulting wire-shaped DSCs could be sealed in a glass capillary (diameter of 0.5 mm). The two electrodes were connected to the external circuit by indium, and the redox electrolyte was finally injected through the capillary force.

4. Characterization. The structures were characterized by TEM (JEOL JEM-2100F operated at 200 kV), AFM (SHIMADZ SPM-9500J3), field-emission scanning electron microscopy (Hitachi FE-SEM S-4800 operated at 1 kV), and

dx.doi.org/10.1021/jp410402w | J. Phys. Chem. C XXXX, XXX, XXX−XXX

Raman spectroscopy (Renishaw inVia Reflex with excitation wavelength of 632.8 nm and laser power of 20 mW). $J-V$ curves were recorded on a Keithley 2400 Source Meter under illumination (100 mW/cm^2) of simulated AM1.5 solar light coming from a solar simulator (Oriel-Sol3A 94023A equipped with a 450 W Xe lamp and an AM1.5 filter). The light intensity was calibrated using a reference Si solar cell (Oriel-91150). Electrochemical impedance spectroscopy (EIS) was carried out by an electrochemical workstation (CHI660a, CH Instruments) in dark. The cyclic voltammetry was performed in an acetonitrile solution containing 0.5 mM I_2, 5 mM LiI, and 0.05 M $LiClO_4$ with a scan rate of 50 mV s^{-1} through a three-electrode setup. For the T^-/T_2 electrolyte, it was composed of 5 mM T^-, 0.5 mM T_2, and 0.1 M $LiClO_4$ in an acetonitrile solution.

RESULTS AND DISCUSSION

Figure 1 has compared the structures of CNT fiber, core–sheath CNT/RGONR fiber, CNT/RGO composite fiber, and RGO fiber by scanning electron microscopy (SEM). These nanostructured fibers shared a uniform diameter of ~33 μm. Figure 1a,b shows SEM images of a bare CNT fiber at different magnifications, and the CNT is highly aligned along the spinning direction. Figure 1c shows SEM image of a core–sheath CNT/RGONR fiber with smoother outer surface compared with the bare CNT fiber. Figure 1d further demonstrates that the CNT is highly aligned in the core and the RGONR sheets are covered on the aligned CNT core to form a thin and uniform sheath. Figure S2 in the Supporting Information shows a representative HRTEM image of a RGONR with width of ~40 nm. In contrast, the CNT/RGO composite fiber exhibits an obvious rippled structure on the surface (Figure 1e). At higher magnification, the CNT remains highly aligned with RGO sheets being connected among them (Figure 1f). The GO sheets exhibited widths ranging from hundreds of nanometers to appropriately 2 μm and an average thickness of ~1.8 nm (Figure S3 in the Supporting Information). Similar to the CNT/RGO composite fiber, a

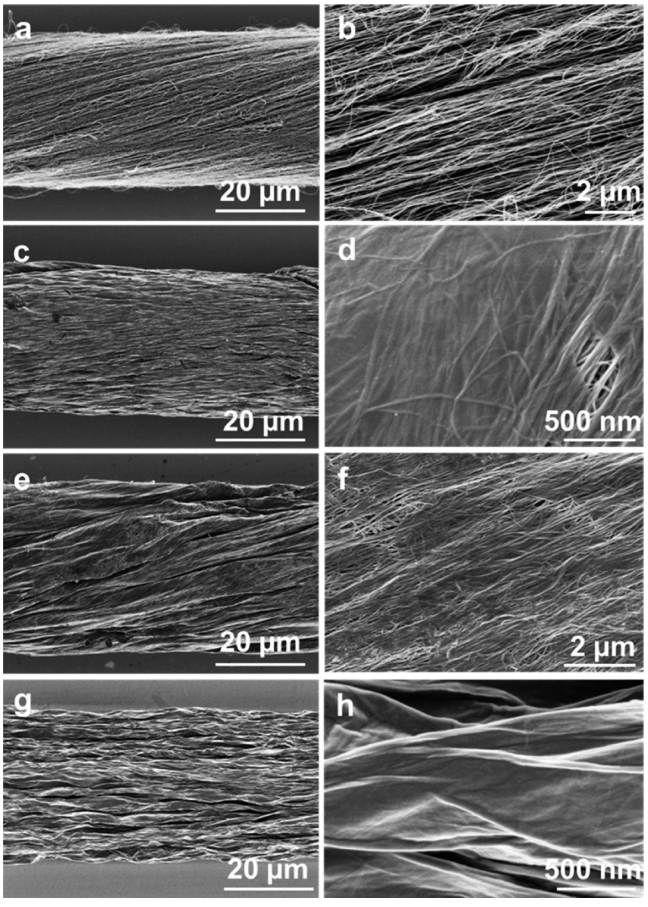

Figure 1. SEM images of CNT fiber, core–sheath CNT/RGONR fiber, CNT/RGO composite fiber, and RGO fiber. (a,b) CNT fiber at low and high magnifications, respectively. (c,d) Core–sheath CNT/RGONR fiber at low and high magnifications, respectively. (e,f) CNT/RGO composite fiber at low and high magnifications, respectively. (g,h) RGO fiber at low and high magnifications, respectively.

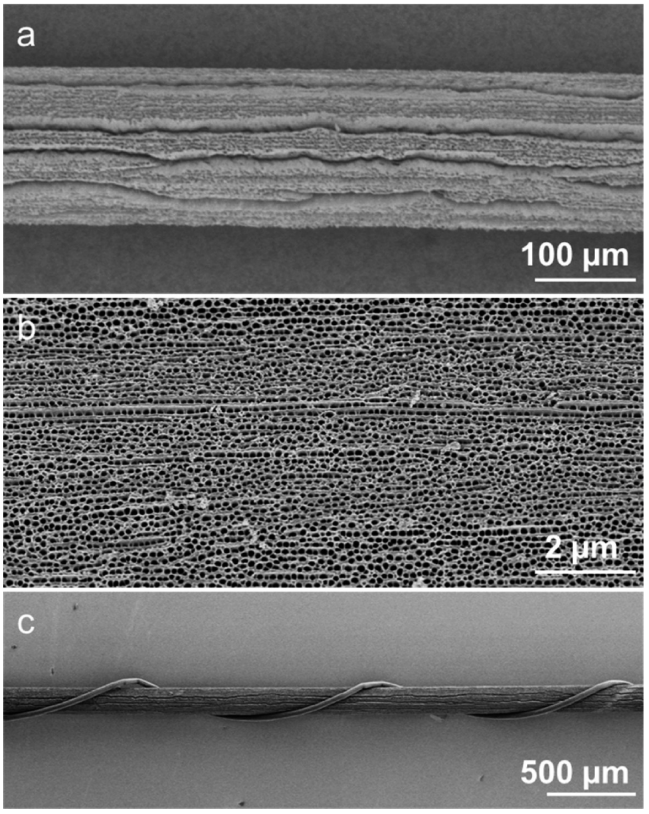

Figure 2. SEM images of the wire-shaped DSCs. (a,b) Electrochemically anodized TiO_2 nanotube arrays on a Ti wire at low and high magnifications, respectively. (c) Typical wire-shaped DSC by twisting a CNT fiber around the anodized Ti wire.

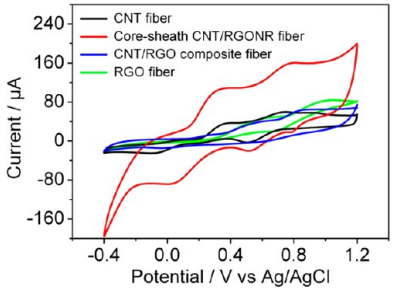

Figure 3. Cyclic voltammograms of CNT fiber, core–sheath CNT/RGONR fiber, CNT/RGO composite fiber, and RGO fiber in the I^-/I_3^- electrolyte. The cyclic voltammetry was performed in an acetonitrile solution containing 0.1 M $LiClO_4$, 5 mM LiI, and 0.5 mM I_2 with a scan rate of 50 mV s^{-1} through a three-electrode setup.

dx.doi.org/10.1021/jp410402w | J. Phys. Chem. C XXXX, XXX, XXX–XXX

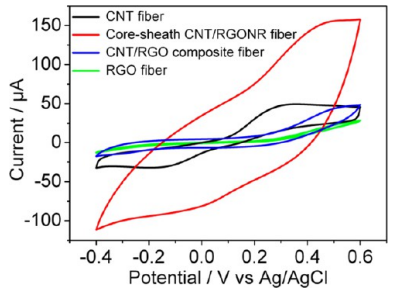

Figure 4. Cyclic voltammograms of CNT fiber, core−sheath CNT/RGONR fiber, CNT/RGO composite fiber, and RGO fiber in the T^-/T_2 electrolyte. The cyclic voltammetry was performed in an acetonitrile solution containing 5 mM T^-, 0.5 mM T_2, and 0.1 M $LiClO_4$ with a scan rate of 50 mV s^{-1} through a three-electrode setup.

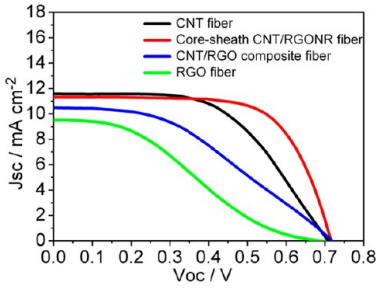

Figure 5. $J-V$ curves of wire-shaped DSCs with CNT fiber, core−sheath CNT/RGONR fiber, CNT/RGO composite fiber, and RGO fiber as counter electrodes in the I^-/I_3^- electrolyte.

bare RGO fiber also shows a rippled structure on the surface (Figure 1g,h).

The working electrodes had been first prepared by electrochemically anodizing Ti wires to fabricate wire-shaped DSCs. Figure 2a,b shows the TiO_2 nanotube arrays formed on the outer surface of the Ti wire. These TiO_2 nanotubes have been perpendicularly aligned, and their diameter and length are (70−100) nm and ∼30 μm,[22] respectively. The TiO_2 nanotubes-modified Ti wire was then wound with the carbon nanostructured fiber to produce a wire-shaped DSC. Figure 2c shows the twisted structure of a typical wire-shaped DSC with a pitch distance of ∼1 mm that had been mainly studied in this work. Although the modified Ti wire working electrode was relatively rigid, the carbon nanostructured fibers were flexible and could be closely twisted with the Ti wire. The resulting good and stable contacts between the two electrodes are important for the rapid charge transportation with high-energy conversion efficiencies and high stability during use.

The CNT fiber, core−sheath CNT/RGONR fiber, CNT/RGO composite fiber, and RGO fiber had been further studied by Raman spectroscopy (Figure S4 in the Supporting Information). All fibers exhibited a D band at ∼1325 cm^{-1} and G band at ∼1585 cm^{-1}. The intensity ratio of the D to G peaks (I_D/I_G) has been generally accepted to reflect the degrees

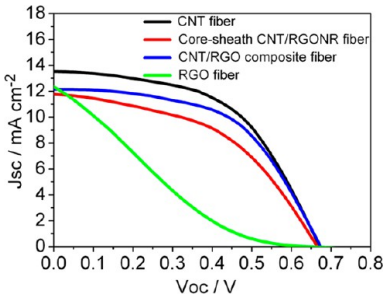

Figure 6. $J-V$ curves of wire-shaped DSCs with CNT fiber, core−sheath CNT/RGONR fiber, CNT/RGO composite fiber, and RGO fiber as counter electrodes in the T^-/T_2 electrolyte.

of graphitizations and defects in carbonaceous materials. The I_D/I_G was 0.91 for the CNT fiber, and it was increased to 1.13 for the CNT/RGO composite fiber as RGO sheets showed low crystallinity with more structural defects than CNT. The I_D/I_G value had been further increased to 1.25 for the core−sheath CNT/RGONR fiber as the Raman spectra were recorded mainly at their outer surfaces, where more RGO sheets had been produced than the CNT/RGO composite fiber. As expected, the bare RGO fiber showed the highest I_D/I_G value of 1.45.

Cyclic voltammetry was first carried out in two different electrolytes under the same condition to study the electrocatalytic activities of four carbon nanostructured fibers. Figure 3 has compared them in the redox couple of I^-/I_3^-, and the cyclic voltammogram of platinum wire is shown in Figure S5 in the Supporting Information. Two typical pairs of redox peaks are observed for these fiber electrodes. The left and right pairs correspond to eqs 1 and 2, respectively.

$$I_3^- + 2e^- \leftrightarrow 3I^- \quad (1)$$

$$3I_2 + 2e^- \leftrightarrow 2I_3^- \quad (2)$$

The left pairs had been generally used to study the electrocatalytic activities of counter electrodes in catalyzing the I_3^- to I^-. A lower peak-to-peak voltage separation (V_{pp}) indicated a higher catalytic activity.[43] Obviously, the core−sheath CNT/RGONR fiber exhibited the lowest V_{pp} value, while the RGO fiber showed the highest V_{pp} value. The V_{pp} values for the CNT fiber and CNT/RGO composite fiber were located between them. Therefore, the catalytic activities for the I^-/I_3^- redox were continuously increased from RGO fiber, CNT/RGO composite fiber, CNT fiber, to core−sheath CNT/RGONR fiber. The highest catalytic activity of the core−sheath CNT/RGONR fiber had been produced by effectively combining the high electrical conductivity in the aligned CNT core and many active edge sites for catalysis in the RGONR sheath. The bare RGO fiber showed the lowest activity due to the low conductivity of ∼150 S/cm compared with ∼310 S/cm of the aligned CNT fiber, ∼380 S/cm of core−sheath CNT/RGONR fiber, and ∼320 S/cm of CNT/

Table 1. Photovoltaic Parameters in Figure 5

counter electrode	V_{OC}/mV	J_{SC}/mA cm^{-2}	FF	η/%
CNT fiber	707	11.56	0.55	4.47
core−sheath CNT/RGONR fiber	713	11.30	0.70	5.64
CNT/RGO composite fiber	714	10.48	0.40	3.02
RGO fiber	683	9.47	0.31	2.02

dx.doi.org/10.1021/jp410402w | J. Phys. Chem. C XXXX, XXX, XXX−XXX

Table 2. Photovoltaic Parameters in Figure 6

counter electrode	V_{OC}/mV	J_{SC}/mA cm^{-2}	FF	η/%
CNT fiber	671	13.47	0.53	4.78
core−sheath CNT/RGONR fiber	664	11.70	0.47	3.70
CNT/RGO composite fiber	672	12.13	0.54	4.42
RGO fiber	641	12.30	0.19	1.46

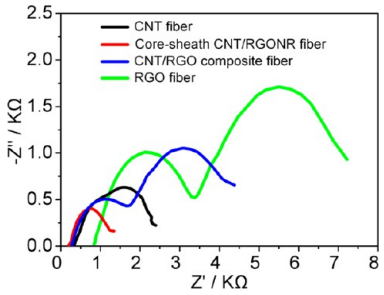

Figure 7. Nyquist spectra of wire-shaped DSCs with CNT fiber, core−sheath CNT/RGONR fiber, CNT/RGO composite fiber, and RGO fiber as counter electrodes in the I^-/I_3^- electrolyte. The frequencies were ranged from 0.1 to 100 kHz with an applied voltage of −0.75 V in dark.

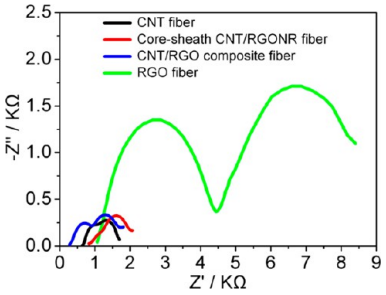

Figure 8. Nyquist spectra of wire-shaped DSCs with CNT fiber, core−sheath CNT/RGONR fiber, CNT/RGO composite fiber, and RGO fiber as counter electrodes in the T^-/T_2 electrolyte. The frequencies were ranged from 0.1 to 100 kHz with an applied voltage of −0.75 V in dark.

RGO composite fiber. Note that the resistances for the RGO fiber, CNT fiber, CNT/RGO composite fiber, and core−sheath CNT/RGONR fiber were ∼3900, 1900, 1800, and 1540 Ω at the same length of 5 cm and radius of 16.5 μm, respectively. The bare RGO fiber that was composed of much larger RGO sheets exhibited less active edges compared with the RGO nanoribbons in the core−sheath CNT/RGONR fiber.

Figure 4 has further compared the four carbon nanostructured fibers in the organic T^-/T_2 redox, and the corresponding cyclic voltammogram of platinum wire is displayed in Figure S6 in the Supporting Information. Typically, a pair of redox peaks had been observed for the redox reaction, that is, $2T^- \leftrightarrow T_2+2e^-$. The obvious redox peaks had been detected for the CNT fiber, and they are not distinct for the core−sheath CNT/RGONR and CNT/RGO composite fibers. In the case of the RGO fiber, almost no redox peaks could be found from the cyclic voltammogram. Increasing catalytic activities were concluded from RGO fiber, core−sheath CNT/RGONR fiber, CNT/RGO composite fiber to CNT fiber for the T^-/T_2 redox. Similar to the I^-/I_3^- redox, the RGO fiber exhibited the lowest activity mainly due to the low conductivity. However, different from the I^-/I_3^- redox, here the CNT fiber showed the highest catalytic activity. It had been found that CNT exhibited higher catalytic activities for the T^-/T_2 redox compared with RGO sheets.[44,45] For the core−sheath CNT/RGONR and CNT/RGO composite fibers, the existence of RGO sheets may hinder the infiltration of the organic T^-/T_2 redox into fibers, so lower catalytic activities were observed.

A series of wire-shaped DSCs had been fabricated by twisting a carbon nanostructured fiber around the modified Ti wire. Figure 5 has compared the $J-V$ curves based on the CNT fiber, core−sheath CNT/RGONR fiber, CNT/RGO composite fiber, and RGO fiber with the I^-/I_3^- electrolyte. The photovoltaic parameters including open-circuit voltage (V_{OC}), fill factor (FF), short-circuit current density (J_{SC}), and photovoltaic conversion efficiency (η) are summarized in Table 1. The core−sheath CNT/RGONR fiber counter electrode showed the highest η of 5.64%. The main difference lied in that the core−sheath CNT/RGONR fiber exhibited much higher FF of 0.70 compared with 0.55 for the bare CNT fiber, 0.40 for the CNT/RGO composite fiber, and 0.31 for the RGO fiber. The above difference can be explained by the highest catalytic activity of the core−sheath CNT/RGONR fiber in the I^-/I_3^- redox, which agrees with the cyclic voltammetry. The corresponding $J-V$ curve based on the platinum wire in this redox couple is displayed in Figure S7 in the Supporting Information. Carbon fiber can be also used as the counter electrode with V_{OC} of 0.725 V, J_{SC} of 6.45 mA cm^{-2}, and FF of 0.57, which produced η of 2.70%.[46]

Figure 6 has also compared $J-V$ curves of the wire-shaped DSCs with the CNT fiber, core−sheath CNT/RGONR fiber, CNT/RGO composite fiber, and RGO fiber as counter electrodes and the organic T^-/T_2 redox couple as the electrolyte. The photovoltaic parameters are summarized at Table 2. The CNT fiber showed a V_{OC} of 671 mV, J_{SC} of 13.47 mA cm^{-2}, and FF of 0.53, which produced the highest η of 4.78%. The CNT/RGO composite fiber shared the same V_{OC} and FF but a little lower J_{SC} of 12.13, which resulted in a lower η of 4.42%. The core−sheath CNT/RGONR fiber demonstrated the same V_{OC} while both lower FF and J_{SC}, and the η value would be calculated as 3.70%. For the RGO fiber, the FF was only 0.19, and the resulting DSC exhibited a much lower η of 1.46%. The energy conversion efficiencies were changed in the same rule as the cyclic voltammetry in the four carbon nanostructured fibers. The platinum wire exhibited an efficiency of 1.98% in the organic redox couple electrolyte (Figure S8 in the Supporting Information).

EIS had been used to investigate these wire-shaped DSCs in dark to further understand the different performances of the four fiber counter electrodes. In the case of the I^-/I_3^- redox electrolyte (Figure 7, Figures S9 and S10 in the Supporting Information), the first semicircle in the Nyquist plot at the high-frequency range corresponded to the impedance at the counter electrode (Rc) for the reduction reaction of I_3^- ions, while the second semicircle at the middle frequency range corresponded to the charge-transfer impedance (Rct) at the interface among the electrolyte, dye, and TiO_2. Obviously, the

dx.doi.org/10.1021/jp410402w | J. Phys. Chem. C XXXX, XXX, XXX−XXX

sizes of the first semicircles were continuously decreased from the RGO fiber, CNT/RGO composite fiber, and CNT fiber to core−sheath CNT/RGONR fiber. In other words, the core−sheath CNT/RGONR fiber showed the highest catalytic activity, and RGO fiber showed the lowest, which is also consistent with the cyclic voltammetry. Figure 8 has further shown the electrochemical impedance spectra of their wire-shaped DSCs in the organic T^-/T_2 redox electrolyte. The Bode plots were further shown in Figure S11 in the Supporting Information. The RGO fiber exhibited the largest size for the first semicircle with the lowest catalytic activity. Figure S12 in the Supporting Information showed the Nyquist spectra and bode plots of wire-shaped DSCs with the Pt wire as counter electrodes in the T^-/T_2 electrolyte.

CONCLUSIONS

In summary, we have fabricated a series of novel wire-shaped DSCs using nanostructured fibers based on CNT or RGO as counter electrodes. The photovoltaic performances of the CNT fiber, core−sheath CNT/RGONR fiber, CNT/RGO composite fiber, and RGO fiber had been carefully compared in two different electrolytes of I^-/I_3^- and T^-/T_2. It was found that the core−sheath CNT/RGONR fiber showed the highest energy conversion efficiency of 5.64% in the I^-/I_3^- electrolyte, while the bare CNT fiber produced the highest energy conversion efficiency of 4.78% in the T^-/T_2 electrolyte. The different catalytic activities had been mainly explored by cyclic voltammetry and Nyquist plot, which may provide useful clues for the development of high-performance wire-shaped energy devices including electrochemical supercapacitors besides DSCs explored in this work.

ASSOCIATED CONTENT

Supporting Information

TEM, AFM, and Raman spectra of fibers and Nyquist spectra and bode plots of wire-shaped DSCs. This material is available free of charge via the Internet at http://pubs.acs.org.

AUTHOR INFORMATION

Corresponding Author

*E-mail: penghs@fudan.edu.cn.

Notes

The authors declare no competing financial interest.

ACKNOWLEDGMENTS

This work was supported by NSFC (91027025, 21225417), MOST (2011CB932503, 2011DFA51330), STCSM (11520701400, 12 nm0503200), Fok Ying Tong Education Foundation, the Program for Professor of Special Appointment at Shanghai Institutions of Higher Learning, and the Program for Outstanding Young Scholars from Organization Department of the CPC Central Committee.

REFERENCES

(1) Chen, T.; Barton, S. C.; Binyamin, G.; Gao, Z. Q.; Zhang, Y. C.; Kim, H. H.; Heller, A. A Miniature Biofuel Cell. *J. Am. Chem. Soc.* **2001**, *123*, 8630−8631.

(2) Heller, A. Miniature Biofuel Cells. *Phys. Chem. Chem. Phys.* **2004**, *6*, 209−216.

(3) Ren, J.; Li, L.; Chen, C.; Chen, X. L.; Cai, Z. B.; Qiu, L. B.; Wang, Y. G.; Zhu, X. R.; Peng, H. S. Twisting Carbon Nanotube Fibers for Both Wire-Shaped Micro-Supercapacitor and Micro-Battery. *Adv. Mater.* **2013**, *25*, 1155−1159.

(4) Lai, W.; Erdonmez, C. K.; Marinis, T. F.; Bjune, C. K.; Dudney, N. J.; Xu, F.; Wartena, R.; Chiang, Y. M. Ultrahigh-Energy-Density Microbatteries Enabled by New Electrode Architecture and Micropackaging Design. *Adv. Mater.* **2010**, *22*, E139−E144.

(5) O'Regan, B.; Gratzel, M. A Low-Cost, High-Efficiency Solar Cell Based on Dye-sensitized Colloidal TiO_2 Films. *Nature* **1991**, *353*, 737−740.

(6) Yoon, J.; Baca, A. J.; Park, S. I.; Elvikis, P.; Geddes, J. B.; Li, L. F.; Kim, R. H.; Xiao, J. L.; Wang, S. D.; Kim, T. H.; et al. Ultrathin Silicon Solar Microcells for Semitransparent, Mechanically Flexible and Microconcentrator Module Designs. *Nat. Mater.* **2008**, *7*, 907−915.

(7) Carlson, D. E.; Wronski, C. R. Amorphous Silicon Solar Cell. *Appl. Phys. Lett.* **1976**, *28*, 671−673.

(8) Hagfeldt, A.; Boschloo, G.; Sun, L. C.; Kloo, L.; Pettersson, H. Dye-Sensitized Solar Cells. *Chem. Rev.* **2010**, *110*, 6595−6663.

(9) Kuang, D.; Brillet, J.; Chen, P.; Takata, M.; Uchida, S.; Miura, H.; Sumioka, K.; Zakeeruddin, S. M.; Gratzel, M. Application of Highly Ordered TiO_2 Nanotube Arrays in Flexible Dye-Sensitized Solar Cells. *ACS Nano* **2008**, *2*, 1113−1116.

(10) Kang, M. G.; Park, N. G.; Ryu, K. S.; Chang, S. H.; Kim, K. J. A 4.2% Efficient Flexible Dye-Sensitized TiO_2 Solar Cells Using Stainless Steel Substrate. *Sol. Energy Mater. Sol. Cells* **2006**, *90*, 574−581.

(11) Ito, S.; Ha, N. L. C.; Rothenberger, G.; Liska, P.; Comte, P.; Zakeeruddin, S. M.; Pechy, P.; Nazeeruddin, M. K.; Gratzel, M. High-Efficiency (7.2%) Flexible Dye-Sensitized Solar Cells with Ti-Metal Substrate for Nanocrystalline-TiO_2 Photoanode. *Chem. Commun.* **2006**, *38*, 4004−4006.

(12) Yella, A.; Lee, H. W.; Tsao, H. N.; Yi, C. Y.; Chandiran, A. K.; Nazeeruddin, M. K.; Diau, E. W. G.; Yeh, C. Y.; Zakeeruddin, S. M.; Gratzel, M. Porphyrin-Sensitized Solar Cells with Cobalt (II/III)-Based Redox Electrolyte Exceed 12% Efficiency. *Science* **2011**, *334*, 629−634.

(13) Lindstrom, H.; Rensmo, H.; Sodergren, S.; Solbrand, A.; Lindquist, S. E. Electron Transport Properties in Dye-Sensitized Nanoporous-Nanocrystalline TiO_2 Films. *J. Phys. Chem.* **1996**, *100*, 3084−3088.

(14) Fang, X. M.; Ma, T. L.; Guan, G. Q.; Akiyama, M.; Kida, T.; Abe, E. Effect of the Thickness of the Pt Film Coated on a Counter Electrode on the Performance of a Dye-Sensitized Solar Cell. *J. Electroanal. Chem.* **2004**, *570*, 257−263.

(15) Murakami, T. N.; Gratzel, M. Counter Electrodes for DSC: Application of Functional Materials as Catalysts. *Inorg. Chim. Acta* **2008**, *361*, 572−580.

(16) Martinson, A. B. F.; Hamann, T. W.; Pellin, M. J.; Hupp, J. T. New Architectures for Dye-Sensitized Solar Cells. *Chem.—Eur. J.* **2008**, *14*, 4458−4467.

(17) Zhang, Z.; Chen, P.; Murakami, T. N.; Zakeeruddin, S. M.; Gratzel, M. The 2,2,6,6-tetramethyl-1-piperidinyloxy Radical: An Efficient, Iodine-Free Redox Mediator for Dye-Sensitized Solar Cells. *Adv. Funct. Mater.* **2008**, *18*, 341−346.

(18) Wang, M. K.; Chamberland, N.; Breau, L.; Moser, J. E.; Humphry-Baker, R.; Marsan, B.; Zakeeruddin, S. M.; Gratzel, M. An Organic Redox Electrolyte to Rival Triiodide/Iodide in Dye-Sensitized Solar Cells. *Nat. Chem.* **2010**, *2*, 385−389.

(19) Wang, Z. S.; Sayama, K.; Sugihara, H. Efficient Eosin Y Dye-Sensitized Solar Cell Containing Br^-/Br_3^- Electrolyte. *J. Phys. Chem. B* **2005**, *109*, 22449−22455.

(20) Li, D. M.; Li, H.; Luo, Y. H.; Li, K. X.; Meng, Q. B.; Armand, M.; Chen, L. Q. Non-Corrosive, Non-Absorbing Organic Redox Couple for Dye-Sensitized Solar Cells. *Adv. Funct. Mater.* **2010**, *20*, 3358−3365.

(21) Tian, H. N.; Jiang, X. A.; Yu, Z.; Kloo, L.; Hagfeldt, A.; Sun, L. C. Efficient Organic-Dye-Sensitized Solar Cells Based on an Iodine-Free Electrolyte. *Angew. Chem., Int. Ed.* **2010**, *49*, 7328−7331.

(22) Pan, S. W.; Yang, Z. B.; Li, H. P.; Qiu, L. B.; Sun, H.; Peng, H. S. Efficient Dye-Sensitized Photovoltaic Wires Based on an Organic Redox Electrolyte. *J. Am. Chem. Soc.* **2013**, *135*, 10622−10625.

(23) Yue, G. T.; Wu, J. H.; Xiao, Y. M.; Lin, J. M.; Huang, M. L.; Lan, Z. Application of Poly(3,4-ethylenedioxythiophene):Polystyrenesulfo-

nate/Polypyrrole Counter Electrode for Dye-Sensitized Solar Cells. *J. Phys. Chem. C* **2012**, *116*, 18057−18063.
(24) Tai, Q. D.; Chen, B. L.; Guo, F.; Xu, S.; Hu, H.; Sebo, B.; Zhao, X. Z. In Situ Prepared Transparent Polyaniline Electrode and Its Application in Bifacial Dye-Sensitized Solar Cells. *ACS Nano* **2011**, *5*, 3795−3799.
(25) Xia, J. B.; Chen, L.; Yanagida, S. Application of Polypyrrole as a Counter Electrode for a Dye-Sensitized Solar Cell. *J. Mater. Chem.* **2011**, *21*, 4644−4649.
(26) Wu, M. X.; Lin, X.; Wang, T. H.; Qiu, J. S.; Ma, T. L. Low-Cost Dye-Sensitized Solar Cell Based on Nine Kinds of Carbon Counter Electrodes. *Energy Environ. Sci.* **2011**, *4*, 2308−2315.
(27) Wang, H.; Hu, Y. H. Graphene as a Counter Electrode Material for Dye-Sensitized Solar Cells. *Energy Environ. Sci.* **2012**, *5*, 8182−8188.
(28) Dubacheva, G. V.; Liang, C. K.; Bassani, D. M. Functional Monolayers from Carbon Nanostructures - Fullerenes, Carbon Nanotubes, and Graphene - As Novel Materials for Solar Energy Conversion. *Coord. Chem. Rev.* **2012**, *256*, 2628−2639.
(29) Wang, Y. D.; Wu, M. X.; Lin, X.; Shi, Z. C.; Hagfeldt, A.; Ma, T. L. Several Highly Efficient Catalysts for Pt-Free and FTO-Free Counter Electrodes of Dye-Sensitized Solar Cells. *J. Mater. Chem.* **2012**, *22*, 4009−4014.
(30) Shang, G. L.; Wu, J. H.; Huang, M. L.; Lin, J. M.; Lan, Z.; Huang, Y. F.; Fan, L. Q. Facile Synthesis of Mesoporous Tin Oxide Spheres and Their Applications in Dye-Sensitized Solar Cells. *J. Phys. Chem. C* **2012**, *116*, 20140−20145.
(31) Zhang, S.; Ji, C. Y.; Bian, Z. Q.; Liu, R. H.; Xia, X. Y.; Yun, D. Q.; Zhang, L. H.; Huang, C. H.; Cao, A. Y. Single-Wire Dye-Sensitized Solar Cells Wrapped by Carbon Nanotube Film Electrodes. *Nano Lett.* **2011**, *11*, 3383−3387.
(32) Liu, D. Y.; Zhao, M. Y.; Li, Y.; Bian, Z. Q.; Zhang, L. H.; Shang, Y. Y.; Xia, X. Y.; Zhang, S.; Yun, D. Q.; Liu, Z. W.; et al. Solid-State, Polymer-Based Fiber Solar Cells with Carbon Nanotube Electrodes. *ACS Nano* **2012**, *6*, 11027−11034.
(33) Wang, X.; Zhi, L. J.; Mullen, K. Transparent, Conductive Graphene Electrodes for Dye-Sensitized Solar Cells. *Nano Lett.* **2008**, *8*, 323−327.
(34) Zou, D. C.; Wang, D.; Chu, Z. Z.; Lv, Z. B.; Fan, X. Fiber-Shaped Flexible Solar Cells. *Coord. Chem. Rev.* **2010**, *254*, 1169−1178.
(35) Chen, T.; Qiu, L. B.; Yang, Z. B.; Peng, H. S. Novel Solar Cells in a Wire Format. *Chem. Soc. Rev.* **2013**, *42*, 5031−5041.
(36) Fan, X.; Chu, Z. Z.; Wang, F. Z.; Zhang, C.; Chen, L.; Tang, Y. W.; Zou, D. C. Wire-Shaped Flexible Dye-Sensitized Solar Cells. *Adv. Mater.* **2008**, *20*, 592−595.
(37) Chen, T.; Qiu, L. B.; Kia, H. G.; Yang, Z. B.; Peng, H. S. Designing Aligned Inorganic Nanotubes at the Electrode Interface: Towards Highly Efficient Photovoltaic Wires. *Adv. Mater.* **2012**, *24*, 4623−4628.
(38) Zhang, S.; Ji, C. Y.; Bian, Z. Q.; Yu, P. R.; Zhang, L. H.; Liu, D. Y.; Shi, E. Z.; Shang, Y. Y.; Peng, H. T.; Cheng, Q.; et al. Porous, Platinum Nanoparticle-Adsorbed Carbon Nanotube Yarns for Efficient Fiber Solar Cells. *ACS Nano* **2012**, *6*, 7191−7198.
(39) Chen, T.; Wang, S. T.; Yang, Z. B.; Feng, Q. Y.; Sun, X. M.; Li, L.; Wang, Z. S.; Peng, H. S. Flexible, Light-Weight, Ultrastrong, and Semiconductive Carbon Nanotube Fibers for a Highly Efficient Solar Cell. *Angew. Chem., Int. Ed.* **2011**, *50*, 1815−1819.
(40) Kosynkin, D. V.; Higginbotham, A. L.; Sinitskii, A.; Lomeda, J. R.; Dimiev, A.; Price, B. K.; Tour, J. M. Longitudinal Unzipping of Carbon Nanotubes to Form Graphene Nanoribbons. *Nature* **2009**, *458*, 872−876.
(41) Yang, Z. B.; Liu, M. K.; Zhang, C.; Tjiu, W. W.; Liu, T. X.; Peng, H. S. Carbon Nanotubes Bridged with Graphene Nanoribbons and Their Use in High-Efficiency Dye-Sensitized Solar Cells. *Angew. Chem., Int. Ed.* **2013**, *52*, 3996−3999.
(42) Yang, Z.; Sun, H.; Chen, T.; Qiu, L.; Luo, Y.; Peng, H. Photovoltaic Wire Derived From a Graphene Composite Fiber Achieving an 8.45% Energy Conversion Efficiency. *Angew. Chem., Int. Ed.* **2013**, *52*, 7545−7548.
(43) Gong, F.; Wang, H.; Xu, X.; Zhou, G.; Wang, Z. S. In Situ Growth of Co(0.85)Se and Ni(0.85)Se on Conductive Substrates as High-Performance Counter Electrodes for Dye-Sensitized Solar Cells. *J. Am. Chem. Soc.* **2012**, *134*, 10953−10958.
(44) Wu, H.; Lv, Z.; Chu, Z.; Wang, D.; Hou, S.; Zou, D. Graphite and Platinum's Catalytic Selectivity for Disulfide/Thiolate (T_2/T^-) and Triiodide/Iodide (I_3^-/I^-). *J. Mater. Chem.* **2011**, *21*, 14815−14820.
(45) Hao, F.; Wang, Z.; Luo, Q.; Lou, J.; Li, J.; Wang, J.; Fan, S.; Jiang, K.; Lin, H. Highly Catalytic Cross-Stacked Superaligned Carbon Nanotube Sheets for Iodine-Free Dye-Sensitized Solar Cells. *J. Mater. Chem.* **2012**, *22*, 22756−22762.
(46) Hou, S. C.; Cai, X.; Fu, Y. P.; Lv, Z. B.; Wang, D.; Wu, H. W.; Zhang, C.; Chu, Z. Z.; Zou, D. C. Transparent Conductive Oxide-Less, Flexible, and Highly Efficient Dye-Sensitized Solar Cells with Commercialized Carbon Fiber as the Counter Electrode. *J. Mater. Chem.* **2011**, *21*, 13776−13779.